Fabrication and Characterization of a Leaky Lens Photo-Conductive Antenna on Low Temperature Grown GaAs Membranes

Bueno, J.; Sberna, P. M.; Fiorellini-Bernardis, A.; Zhang, H.; Neto, A.; Llombart, N.

DOI
10.1109/TTHZ.2023.3281770

Publication date
2023

Document Version
Final published version

Published in
IEEE Transactions on Terahertz Science and Technology

Fabrication and Characterization of a Leaky-Lens Photoconductive Antenna on Low-Temperature Grown GaAs Membranes

Juan Bueno, Paolo Maria Sberna, Arturo Fiorellini-Bernardis, *Student Member, IEEE*, Huasheng Zhang, *Graduate Student Member, IEEE*, Andrea Neto, *Fellow, IEEE*, and Nuria Llombart, *Fellow, IEEE*

***Abstract*—State-of-the-art THz pulsed commercial systems operating over large bandwidth suffer from high dispersion or low radiation efficiency due to the poor coupling between the transmitter and receiver photoconductive antennas (PCAs). In this work, we present the fabrication and characterization of a leaky-lens PCA that has the potential to solve this problem. The presented PCA is based on a low-temperature grown gallium arsenide (LT-GaAs) membrane with a 1:15 bandwidth coverage (0.1–1.5 THz), where the frequency response is constant. In order to fabricate the PCA on an LT-GaAs membrane, a novel fabrication process is developed. This process is dramatically faster than previously used processes (∼1.5 h instead of ∼20 h). Furthermore, an experimental validation of the radiated power together with the comparison to a standard bow–tie-based PCA fabricated on the same LT-GaAs wafer is shown in this article. We show that the PCA source on the LT-GaAs membrane is more efficient due to the enhanced leaky wave radiation. The leaky-lens PCA stands out as a great candidate to improve the coupling efficiency in THz pulsed commercial systems, where the maximum laser power that can be used is limited by the dispersion in the optic fiber.**

***Index Terms*—Leaky-lens antenna, membrane-based micro-antenna, photoconductive antenna (PCA), THz radiation, time-domain spectroscopy.**

I. Introduction

THE THz time-domain sensing and spectroscopy (TDSS) systems are nowadays employed for multiple applications, such as chemistry, solid-state physics, and industrial process monitoring [1], [2], [3], [4], [5], [6], [7], [8]. Current TDSS commercial systems are based on single planar antenna geometries, printed on a photoconducting substrate, where the electrically small gap of the antenna is periodically (80–100 MHz) shined by a femtoseconds (∼100 fs) laser pulse with a wavelength matched to the semiconductor energy gap. The pulse injects electrons from the valence to the conduction band of the semiconductor. The photocarriers are accelerated by the bias voltage between the antenna electrodes; hence, a transient photocurrent is generated in the photoconductive antenna (PCA). The intensity and the frequency spectrum of the photocurrent is a function of the optical and electrical properties of the semiconductor [5]. The transient photocurrent, then, releases a part of its energy as radiated electromagnetic field [9]. However, the spectrum of the field arriving at the receiver antenna not only depends on the emitter photocurrent spectrum but also on the following:

1) the photoconductive source–antenna matching problem;
2) the coupling between the PCA chip and the HR Si lens (dispersion problem);
3) the quasi-optical (QO) propagation channel efficiency (THz radiation spillover and dispersion problem).

To the best of our knowledge, the efforts in the THz community are mainly focused on the engineering of the semiconductor properties, e.g., carrier scattering and life time, through materials synthesis and postprocessing [10], [11]. On the other hand, significant performance improvement can be also achieved focusing on the antenna architecture and its radiation properties [8], [12], [13].

The most common antenna geometries used in the dawn of PCA research are Auston switches (or H-dipoles) [3], bow–tie antennas [14], and strip line antennas [15], and they have been thoroughly studied and compared [7]. These types of antennas are still being used in current TDSS systems nowadays. Other types of antennas have been also used and studied. A good review can be found in [16]. It has been shown the importance of the antenna geometry for enhancing the radiation properties of PCAs [17], where it was already proposed the use of leaky-lens architectures based on the printed slots in a micrometric membrane in order to illuminate the lens more efficiently and improve the QO channel efficiency. Specifically, the introduction of a small (in terms of wavelength) air gap between the metallization and the lens is sufficient to enable broadband leaky radiation toward the lens vertical axis [17]. This gap is used to achieve a more directive radiation inside the silicon medium and, therefore, illuminate more efficiently only the top of the lens [18]. This leaky-lens antenna, characterized by a stable radiation

Manuscript received 7 December 2022; revised 3 April 2023 and 6 May 2023; accepted 23 May 2023. Date of publication 31 May 2023; date of current version 5 September 2023. This work was supported by ERC Starting Grant LAA-THz-CC under Grant 639749. *(Corresponding author: Juan Bueno.)*

Juan Bueno is with the Delft University of Technology, 2628 CD Delft, The Netherlands (e-mail: j.buenolopez@tudelft.nl).

Paolo Maria Sberna is with the Else Kooi Laboratory, Delft University of Technology, 2628 CD Delft, The Netherlands (e-mail: p.m.sberna@tudelft.nl).

Arturo Fiorellini-Bernardis, Huasheng Zhang, Andrea Neto, and Nuria Llombart are with the Delft University of Technology, 2628 CD Delft, The Netherlands (e-mail: a.fiorellinibernardis@tudelft.nl; h.zhang-12@tudelft.nl; a.neto@tudelft.nl; n.llombartjuan@tudelft.nl).

Color versions of one or more figures in this article are available at https://doi.org/10.1109/TTHZ.2023.3281770.

Digital Object Identifier 10.1109/TTHZ.2023.3281770

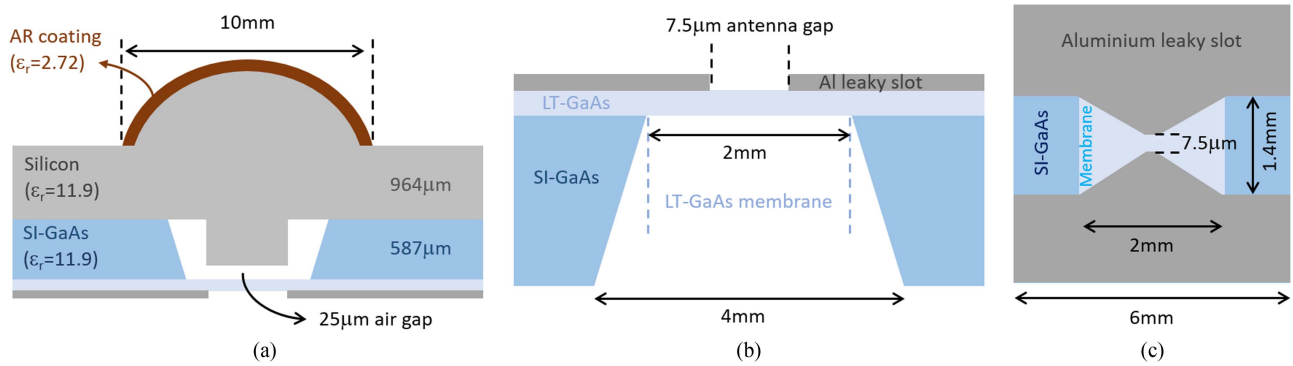

Fig. 1. (a) Sketch (not to scale) of the leaky-lens PCA, including the silicon lens. (b) Cross section of the LT-GaAs membrane. (c) Top view of the LT-GaAS membrane showing the leaky-lens slot and excitation gap.

phase center, improves the coupling between the PCA radiation with the QO channel.

In this contribution, we demonstrate, for the first time, the realization of a PCA based on a leaky-lens antenna architecture experimentally, with a novel manufacturing technique that allows the creation of suspended LT-GaAs membranes with thicknesses of a few μm, and theoretically, with the use of the theoretical circuit model introduced in [9] and [13] to evaluate the radiated power. We compare the performance of the leaky-lens PCA with the state-of-the-art bow–tie PCA, which performs better than the commonly used H-dipole antennas [12]. Both antennas are fabricated from the same wafer and in the same processing run, and they both have the same bias and optical conditions. We demonstrate that leaky-lens PCA outperforms the bow–tie-based PCA in terms of QO channel efficiency, disclosing the full potential of leaky-lens PCAs for fiber-coupled THz TDSS systems.

II. Enhanced Leaky PCA and Antenna Performance

The proposed PCA is based on a leaky-lens antenna [18] integrated with a silicon hemispherical lens, as shown in Fig. 1(a). The hemisphere lens has a diameter of 10 mm and the extension of 1.551 mm. A quarter-wavelength matching layer (at frequency 0.4 THz) is deposited on the top of the lens surface to improve the transmission between the air–silicon interface. Parylene-C, whose relative permittivity is 2.72, with a thickness of 114 μm is used as the matching layer [19]. The silicon lens is illuminated by a tapered slot through an air cavity with a thickness of 25 μm. The LT-GaAs suspended membrane occupies the central square area of the chip, with the bow–tie slot gap at its center. The membrane is a square of $\sim$2.2 mm sides and 2 μm thick [see Fig. 1(b)]. The leaky slot metallization resembles a bow–tie with a 55° taper and a square gap of 7.5 μm at the center of the slot. The dimensions of the bow–tie are 1.4 mm long and 2 mm wide. The contact pads extend beyond, for a total chip size of 6 $\times$ 6 mm [see Fig. 1(c)]. All the chip front surfaces, except for the contact pads, have been covered with 2.6 μm thick amorphous fluoropolymer (Cytop from AGC Chemicals) in order to provide a better mechanical strength to the LT-GaAs membrane and to passivate its surface against the formation of moisture layer, also preventing a potential electrical breakdown of the LT-GaAs during high-voltage operation.

The antenna structure in Fig. 1(a) is simulated using CST, a full-wave EM software [20], where the lens is replaced by semi-infinite silicon medium. The simulated antenna impedance is shown in Fig. 2(a), together with the impedance of a standard bow–tie antenna, taken from the article presented in [13], for comparison. The impedance of the leaky-lens antenna is higher than that of the bow–tie antenna and it varies more significantly versus frequency.

Leaky-lens antennas are particularly efficient at illuminating dielectric lenses, and their radiation patterns are much more focused when compared with a standard bow–tie antennas [17]. The fields radiated by the leaky-lens antenna into the infinite silicon medium (primary fields) are shown in Fig. 2(d)–(f) at 0.1 THz, 0.5 THz, and 1 THz, respectively, and compared with the patterns of a standard bow–tie antenna, such as the one in [13]. The patterns show a typical leaky radiation, which are more symmetric and more focused at broadside than the patterns of the bow–tie.

The primary fields are then transmitted outside the extended hemispherical lens. The lens radiation efficiency is obtained by integrating these transmitted fields on the lens surface and divided by the antenna radiated power, and it is shown in Fig. 2(d) as a function of frequency for both antennas. This efficiency considers the spillover of the antenna feed and the reflection at the lens surface. As expected, the leaky-lens antenna illuminates the lens more efficiently than the bow–tie antenna because of its more directive primary patterns. The frequency oscillation is the result of the adoption of a single matching layer that is tuned to maximize the efficiency at 400 GHz and multiples.

The fields radiated by this leaky-lens antenna (secondary fields) are evaluated using an in-house physical optics (PO) code [21]. The patterns are evaluated on a far-field sphere (1 m) from the phase center of the lens, which is 15.8 mm below the slot metallization. Fig. 2(g)–(i) shows these patterns at 0.1 THz, 0.5 THz, and 1 THz, respectively. The corresponding gain versus frequency is shown in Fig. 2(c) and includes the radiation efficiency of the lens antenna [see Fig. 2(b)]. At low frequencies ($\leq$ 0.1 THz), the patterns of the leaky and the bow–tie antennas are similar, which are well-focused toward broadside. However, as the frequency increases, the patterns of the bow–tie antenna are becoming more distorted and non-broadside, and have unwanted radiation at around 10°. As the result, the gain of the bow–tie antenna drops around 0.35 THz and remains almost

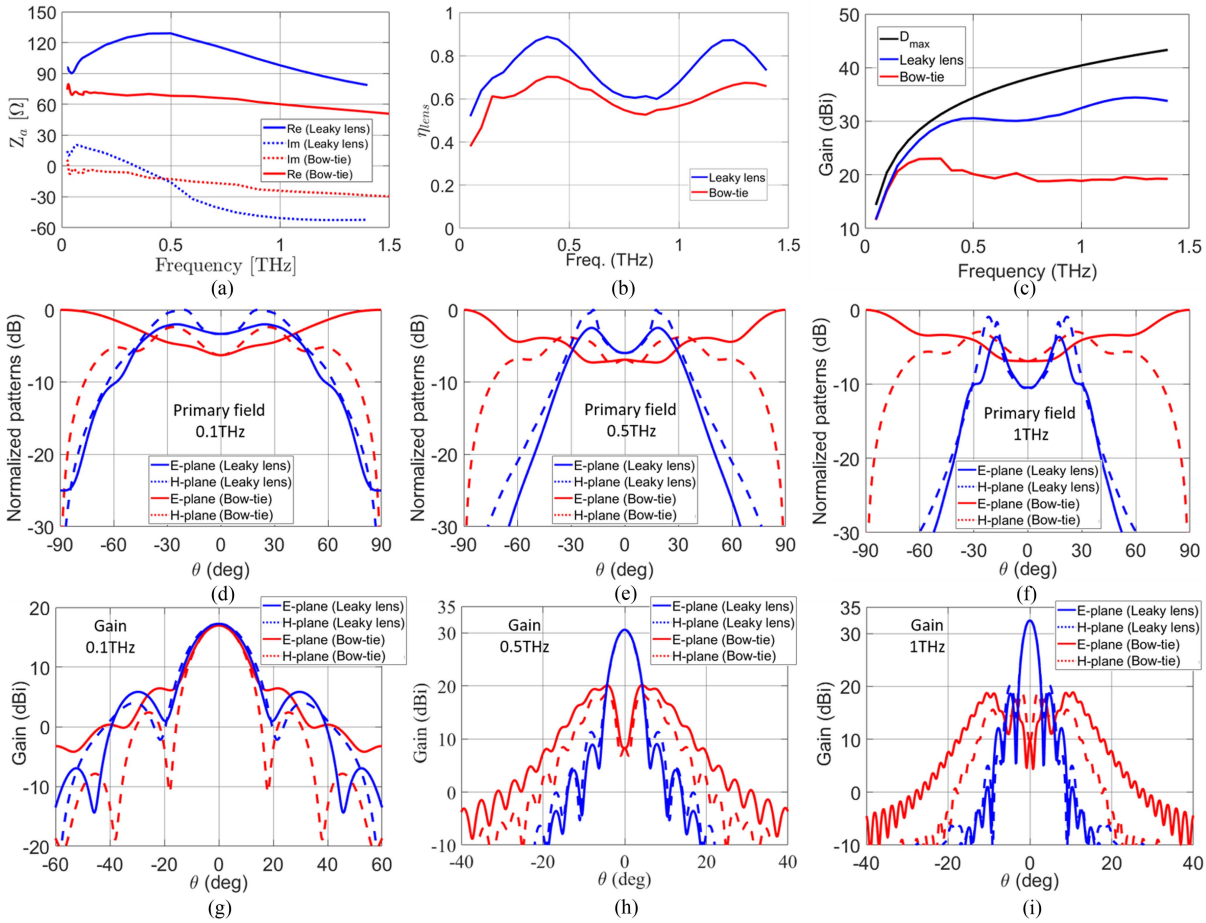

Fig. 2. Antenna-simulated performance for the proposed leaky slot and the bow–tie from the article presented in [13]. (a) Input impedance. (b) Lens radiation efficiency. (c) Antenna gain. (d)–(f) Primary fields radiated into an infinite silicon medium at 0.1 THz, 0.5 THz, and 1 THz, respectively. (g)–(i) Antenna gain in the far field at 0.1 THz, 0.5 THz, and 1 THz, respectively.

TABLE I
COMPARISON AMONG STATE-OF-THE-ART FIBER-FED COMMERCIAL LENS-COUPLED PCAS

Antenna type	λ (nm)	Material	P_{laser} (mW)	V_{bias} (V)	P_{THz} (μW)
Auston [Menlo - 24]	1560	Fe:InGaAs	30	100	60
Strip line [Toptica - 25]	1560	InGaAs	20	100	70
Bow–tie [TUD - 13]	780	LT-GaAs	42	30	65
Leaky lens [this work]	780	LT-GaAs	24	30	65

constant after that. While the gain of the leaky-lens antenna keeps increasing versus frequency and is much larger than the one of the bow–tie antenna. The maximum achievable directivity for the given lens diameter is shown as the black line in Fig. 2(c).

A comparison between commercially available optical fiber-fed PCAs and the leaky-lens antenna is shown in Table I. It can be seen that the leaky-lens antenna emits the same THz power that the Auston switch antenna from Menlo Systems [22] and the strip line antenna from Toptica Photonics [23] with a similar laser excitation but with a lower voltage bias. We add the bow–tie antenna [13] to this table because we can directly simulate, measure, and compare the results much easily to the leaky-lens antenna since it is our own design. The reason why the leaky lens generates the same THz power than the other antennas at a lower voltage bias is that the leaky lens couples more efficiently to the QO channel.

III. FABRICATION OF THE LT-GAAS MEMBRANE-BASED PCA

The enhancement of the broadside radiation via leaky-lens slot is achieved, thanks to its realization on a suspended membrane. We use a thin membrane of photoconductive low-temperature grown GaAs as the slot substrate. Previous work shows that dry (i.e., plasma) etching has an intrinsic limitation in the maximum etched depth, setting it to a hundred of micrometers. This is due to the fact that Ga fluoride, chloride, and bromide generated as byproducts during the plasma etching have very high vapor pressures. Thus, the etching is strongly limited by their desorption from the surface and, as a consequence, it is extremely hard, if not impossible, to etch hundreds of microns-thick GaAs substrates. Alternatively, GaAs trenches

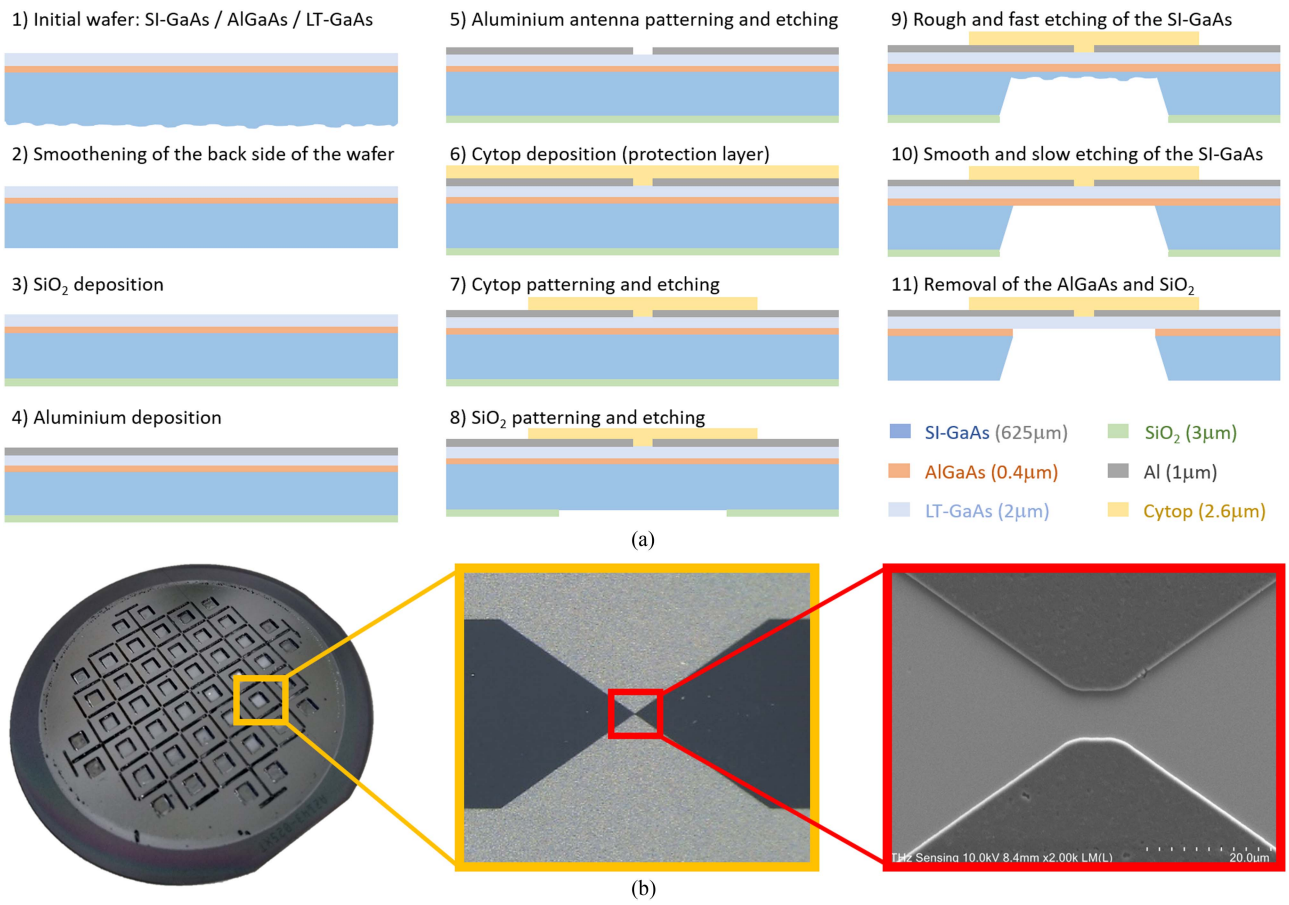

Fig. 3. (a) Schematic drawing (not to scale) of the process flow. A detailed description of the fabrication process can be found in the text. (b) Images of the fabricated wafer. Left: Optical image of the back side of the wafer where all the membranes are etched. Middle: Optical image of the front side of the wafer where the leaky-lens PCA is fabricated. Right: Scanning electron microscope (SEM) image of the antenna gap of the leaky-lens PCA.

deeper than hundreds of microns can be etched by means of wet etches based on citric acid [24], [25].

For the procedure adopted in this work, we developed a selective wet etch based on NH_4OH/H_2O_2 mixtures. The wet etching of GaAs in NH_4OH/H_2O_2 mixtures is highly crystallographic, as the relative etch rate of the crystalline planes follows this order: $[111]_{\text{As rich}} > [100] > [110] > [111]_{\text{Ga rich}}$ [20]. The specific etching ratio depends on the specific NH_4OH/H_2O_2 ratio [26]. Due to this etch rate difference, the walls of the membrane cavity assumed a tapered shape, which is not relevant for the properties of our leaky-lens antennas. The etching method is similar to the one reported in [24] and [25], where the authors employ a citric acid/H_2O_2 mixture instead of NH_4OH/H_2O_2 mixtures. However, in our case, the etching is dramatically faster, taking $\sim$1.5 h instead of $\sim$20 h.

The leaky-lens PCA is manufactured from a 3 in diameter and 625 μm thick semi-insulating (SI) single-crystalline GaAs wafer. A multilayer consisting of 0.2 μm thick GaAs, 0.4 μm thick $Al_{0.75}Ga_{0.25}As$, and 2 μm thick LT-GaAs is deposited by molecular beam epitaxy on the front side of the SI-GaAs wafers (see step 1 in Fig. 3). The GaAs layer serves as a buffer layer to accommodate the growth of the $Al_{0.75}Ga_{0.25}As$ film, which acts as the sacrificial etch-stop layer for the membrane release process. The LT-GaAs layer constitutes the photoconductive substrate of the active membrane for the leaky-lens antenna. These layers are grown by the University of Leeds. The front side of the wafer (LT-GaAs) is polished and the back side of the wafer (SI-GaAs) is rough (see step 1 in Fig. 3) and has to be chemically polished to obtain all over the back surface a uniform and constant etching during the membranes release. This polishing ensures that the different crystal facets of the rough surface are smoothened out, making the crystallographic nature of the bulk etching less a risk for etch stop of non-homogeneity.

The fabrication of the leaky-lens antenna chips is performed at the Else Kooi Laboratory at the Delft University of Technology. The fabrication process starts with the cleaning of the wafer from organic contamination, removal of the GaAs native oxide, and chemical polishing of wafer back side. The cleaning and removal of the native oxide is done by soaking the wafer at room temperature first in acetone, then in isopropanol and to conclude in NH_4OH (28% bath). The wafer back-side polishing is performed by immersing the wafer in an NH_4OH (28%) and an H_2O_2 (31%) bath mixed at a 1:2 volume ratio at room temperature for 5 min (see step 2 in Fig. 3). After this procedure, we inspect the back of the wafers under a microscope to be sure that it results smooth and optically polished. The wafer is afterward soaked in NH_4OH (28%) for 5 min.

Next, a 3 μm thick, low-temperature, plasma-enhanced chemical vapor deposited (PECVD) SiO_2 layer, with a compressive stress <150 MPa, is deposited on the back of the wafer (see step 3 in Fig. 3). This SiO_2 layer will be patterned later in the process to define the future location of the membranes.

The antenna metallization layer is realized through dc sputtering at room temperature. A 1 μm thick aluminum (99.999% purity) layer is deposited on top of native oxide-free LT-GaAs surface in an Ar atmosphere (see step 4 in Fig. 3). The LT-GaAs native oxide has been stripped dipping the wafer in an NH_4OH (28%) solution at room temperature for 5 min just before the deposition. The deposition at room temperature serves to avoid any uncontrolled annealing and/or interdiffusion-induced variation of the LT-GaAs electrical properties.

Later, the Al is patterned to realize the desired antenna geometry, as well as the pads for the biasing of the structure (see step 5 in Fig. 3). The Al is etched by a double-step etching, first dry etching and a soft wet landing, to maintain intact the pristine LT-GaAs surface quality, important for the charge carriers recombination at the surface and the overall mechanical stability of the LT-GaAs membrane. The etching of the first 0.8–0.9 μm is done in an inductively coupled plasma reactive ion etching (ICP-RIE) reactor, using a Cl_2/HBr gas mixture and photoresist as the mask. The remaining 0.1–0.2 μm of Al are later removed by wet etching in diluted (10% vol.) NH_4OH that, contrary to the Cl-based RIE, is harmless for the LT-GaAs surface.

A 2.6 μm thick layer of Cytop [27], a transparent fluoropolymer with a refractive index of 1.34 that does not affect the laser absorption in the gap of the antenna, is spun coated on the front side of the wafer and cured on a hot plate (30 min at 80 °C first and then 60 min at 200 °C) in air (see step 6 in Fig. 3). The Cytop layer is patterned, with photoresist as mask, by plasma etching in a RIE reactor with O_2 gas to expose the antenna Al contact pads for wire bonding (see step 7 in Fig. 3). The Cytop coating and etching do not have any impact on the LT-GaAs and Al properties, yet it protects the PCA surface from external agents adsorption (e.g., moisture) while providing mechanical support to the LT-GaAs membrane.

The LT-GaAs membrane is fabricated with a double-step wet etching of the SI-GaAs substrate using, subsequently, two NH_4OH/H_2O_2 mixtures. We use HF-patterned low-T PECVD SiO_2 film as the hard mask on the wafer backside (see step 8 in Fig. 3). The back-to-front alignment accuracy is determined by the mask aligner and is better than 5 μm. In any case, the membrane is over dimensioned by 1 mm on each side and the possible back-to-front misalignment does not have any effect in the antenna performance. During the whole wet etching process, the LT-GaAs side is protected from the aggressive chemical solutions using a PEEK holder from A.M.M.T. [28]. The first etching step is done soaking the wafer in a solution of NH_4OH (28% vol.) and H_2O_2 (31% vol.), mixed at a volume ratio of 1:2 (see step 9 in Fig. 3). This is the same solution that we use to polish the back side of the wafer. The etch rate of this solution is ~8 μm/min and is able to remove the major portion of the substrate much faster than the citric acid solution. An important point to take into consideration is that some etching reaction products, such as $Ga(OH)_3$, are not very soluble in water [29], and they tend to form a reaction-limiting stain on the surface under etching. Thus, it is necessary to constantly stir the solution to have a uniform etching of the GaAs substrate. However, as reported in [24], this mixture is not selective with any AlGaAs alloy. Therefore, the last 50 μm of the substrate are etched using a volume ratio of 1:30 (see step 10 in Fig. 3). This solution has an etch rate of 2 μm/min, roughly four times slower than the previous one, but shows a great selectivity for the $Al_{0.75}Ga_{0.25}As$ layer (etching ratio of at least 100 [24]). Indeed, when the relative amount of the peroxide is that high, the etching of $Al_{0.75}Ga_{0.25}As$ is slowed down by the formation of quasi-passivating Al oxide [24]. The $Al_{0.75}Ga_{0.25}As$ layer is eventually removed, together with the SiO_2 mask, by soaking the wafer in buffered (1:7) HF at room temperature for 20 min (see step 11 in Fig. 3), which is harmless for the LT-GaAs layer.

IV. Assembly of the Membrane-Based PCA

To create the 3-D structure required for the operation of the leaky-lens antenna, we use a very similar assembly to the one used by Garufo et al. [8]. The alignment and the gluing procedure is identical since the same setup is used. The only difference is that the lens design is different in order to create the air gap between the antenna feed and the lens. The lens design is depicted in Fig. 1(a). This lens has a protrusion at the flat side of the lens shape. This protrusion goes inside the membrane cavity at the back of the SI-GaAs wafer and is used to create the air gap. In order the assure that this gap has the correct dimension, the membrane cavity depth is measured accurately with a confocal microscope. The length of the protrusion of the lens is machined accordingly to have a 25 μm gap between the antenna feed and the lens. The depth of the membrane opening is 586±5 μm depending on the position of the cavity in the wafer. The lens is made out of a high resistivity (>10 kΩ·cm) silicon ingot using single-point diamond turning [30] and is fabricated after measuring the membrane cavity depth. The length of the protrusion is chosen to be 561 ± 5 μm to assure the a 25 μm air gap.

V. Experimental Validation

We assess the performance of the leaky-lens PCA presented in this contribution in the THz Laser Laboratory of the Tera-Hertz Sensing Group at TU Delft and compare it with that of a standard bow–tie-based PCA [13] fabricated in the same LT-GaAS wafer. The setup adopted for the measurements is shown in Fig. 4 and is similar to what used in [13]. The free-space laser source used to excite the PCAs is a part of the commercial system TERA K15 from Menlo Systems GmbH [31], which operates at λ = 780 nm and is pulsed at $f_L = 80$ MHz. The PCAs are biased to a fixed voltage V_b, which accelerates the photocarriers injected by the laser source. The induced pulse of photocurrent generates a radiation that is collected by a horn antenna (VDI, CH-WR10) connected to a power meter (VDi, PM5) [32]. The PCAs under investigation are coupled to a horn antenna through a QO path consisting of two identical planoconvex polymer lenses from the TERA K15 system [31].

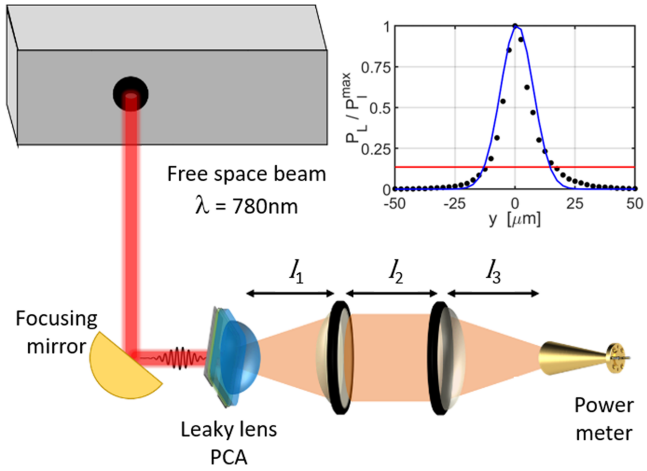

Fig. 4. Sketch (not to scale) of the measurement setup. The leaky-lens PCA is excited by the free-space laser focused by an OFF-axis parabolic mirror. The field radiated is coupled to the receiving horn connected to a power meter via two polymer lenses. The inset (top right) shows the profile of the optical beam focused on the leaky slot gap. The solid blue line is a Gaussian fit to verify the gaussicity of the focused beam. The 3 dB diameter of the beam along the two perpendicular axis is 11.9 μm and 12.7 μm.

A. Experimental Setup

The laser beam exits the TERA K15 and is focused onto the gap in the leaky-lens slot using a gold 90° off-axis parabolic mirror with a reflected focal length of 15 mm (ThorLabs, MPD00M9-M01) [33] to focus the beam down to the desired value. This parabolic mirror is placed at ∼40 cm from the laser output, where the beam still stays collimated. The pulse has a Gaussian temporal profile with a full width at half maximum of $\tau_p = 100$ fs and the average power P_L ranges from 1 to 100 mW. The beam emerges with a 1/e waist of $w_o = 0.6$ mm and is focused down to a waist of $w_L = 6.4$ μm (which corresponds to a -3 dB radius of $r_L^{-3\text{ dB}} = 3.75$ μm or diameter of $D_L^{-3\text{ dB}} = 2 \times r_L^{-3\text{ dB}} = 7.5$ μm) to match the PCA gap lateral dimensions.

To verify the laser profile and the alignment, we measure the profile of the focused beam on both the horizontal and vertical axes using two metal blades and the knife-edge technique [34]. The blades are placed in a holder controlled by a five-axis (three translational and two rotational axis) motorized stage with a translational resolution of $\delta_t = 1.25$ μm and a rotational resolution of $\delta_r = 0.01°$. The holder of the blade is the same one used for the antenna, thus ensuring that the measured profile is eventually the same exciting the investigated PCA. The -3 dB diameter of the beam along the both orthogonal axis is $D_L^v = 11.9$ μm and $D_L^h = 12.7$ μm, respectively. The profile of the laser beam of the vertical axes is shown in the inset on the top right in Fig. 4. It turns out to be extremely difficult to obtain the ideal -3 dB beam diameter using a parabolic mirror. The best alignment we obtained with this setup did not match the ideal -3 dB diameter of 7.5 μm. The aberration given by the focusing mirror introduces an asymmetric tail in the vertical plane. The measured spillover efficiency is $\eta_{\text{SO}}^v \simeq 0.42$ and $\eta_{\text{SO}}^h \simeq 0.34$ on the vertical and horizontal axis, respectively, for an average spillover efficiency of $\eta_{\text{SO}} \simeq 0.38$.

B. Detected Power

Once the desired optical beam profile is achieved, the blades are replaced by the leaky-lens PCA. The position of the leaky-lens PCA is fine-tuned biasing the antenna measuring the dc current induced in the gap by maximizing it using micrometrical position adjustments controlled by the five-axis stage. The position of the two lenses and the horn of the QO path are fine-tuned as well to maximize the power received by the power meter. The distance among the leaky-lens PCA, the lenses, and the power meter is $l_1 = 35$ mm, $l_2 = 60$ mm, and $l_3 = 20$ mm (see Fig. 4). The power collected by the power meter is characterized as a function of the optical power. The PCA is biased to a voltage potential, which is swept at $V_b = 10$, 20, and 30 V. The THz power measured by the PM5 is shown in Fig. 5 and compared with the THz power measured using a bow–tie PCA (with a 10 μm slot gap) under the same biasing conditions [13]. The distance among the bow–tie PCA, the lenses, and the power meter is kept the same since we want to prove that the difference in the detected power between the leaky-lens and the bow–tie antennas is mainly related to the radiation properties and the coupling between them and the QO channel. The leaky-lens antenna achieves a higher QO channel efficiency, as can be seen in Fig. 6(b), because of its more directive secondary fields and higher gain than the bow–tie antenna (especially at high frequencies) when coupling to the QO channel.

The power is expressed as a function of the laser power absorbed by the gap of the antennas P_{gap}. Specifically, P_{gap} relates to the total power being absorbed by the LT-GaAs. This absorbed power relates to the laser output power through the optical efficiency as $P_{\text{gap}} = \eta_{\text{opt}} P_L$, where P_L is the laser output power and η_{opt} accounts for the spillover of the beam over the PC gap, its absorption in the vertical axis, and its reflection efficiency [13]. The optical efficiency is different for both antennas, $\eta_{\text{opt}} = 0.24$ for the leaky-lens PCA, whereas $\eta_{\text{opt}} = 0.35$ for the bow–tie PCA of the article presented in [13] because of its larger slot gap.

It can be observed in Fig. 5 that the increase of the average power of the pulsed laser does not lead to a proportional increase of the THz detected power for any of the two PCAs. For larger optical excitations, a power saturation effect becomes manifest, and it appears to occur faster for the leaky-lens PCA than the bow–tie PCA. Moreover, it is apparent that, at any given bias voltage and laser power, more power is detected for the leaky-lens PCA up to saturation.

C. Comparison Between Measurements and Simulations

We can now use the model proposed in [12] and [13] to understand the difference in detected power between the two PCAs. With this model, we can predict the detected power, including the PCA radiation mechanism as well as the QO channel. The average power detected by the PM5 can be estimated as follows:

$$P_{RX} = 2 f_L \int_0^\infty \text{Re}\{Z_a(f)\} |I_{\text{rad}}(f)|^2 \eta_{qo}(f)\, df \quad (1)$$

where the integration is performed with unilateral spectra. We refer to the article presented in [13] for the detailed derivation of $I_{\text{rad}}(f)$. The antenna radiation impedance, $Z_a(f)$, is the one shown in Fig. 2(a). The impedance of the leaky-lens PCA is

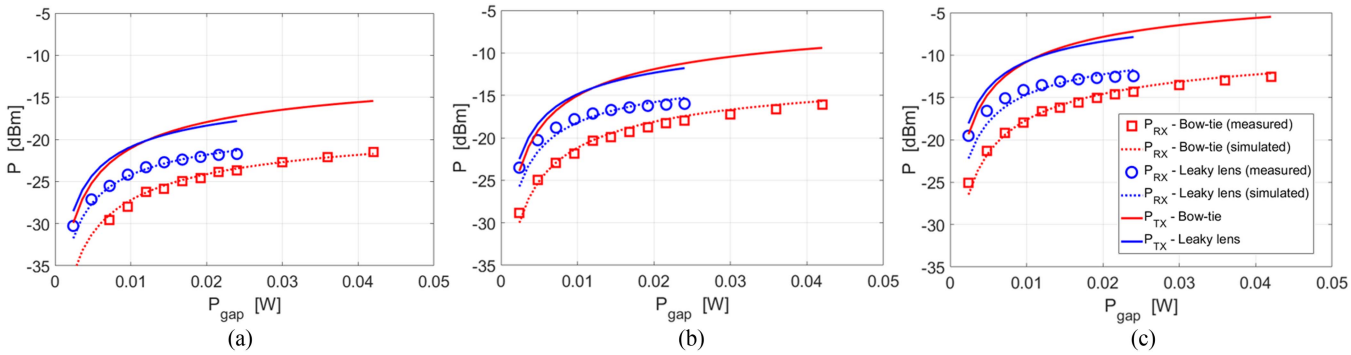

Fig. 5. Detected THz power from leaky-lens and the bow-tie PCAs for three different bias levels as a function of the optical power absorbed in the PCA gap, together with the predicted power. (a) Bias voltage $V_b = 10$ V. (b) Bias voltage $V_b = 20$ V. (c) Bias voltage $V_b = 30$ V.

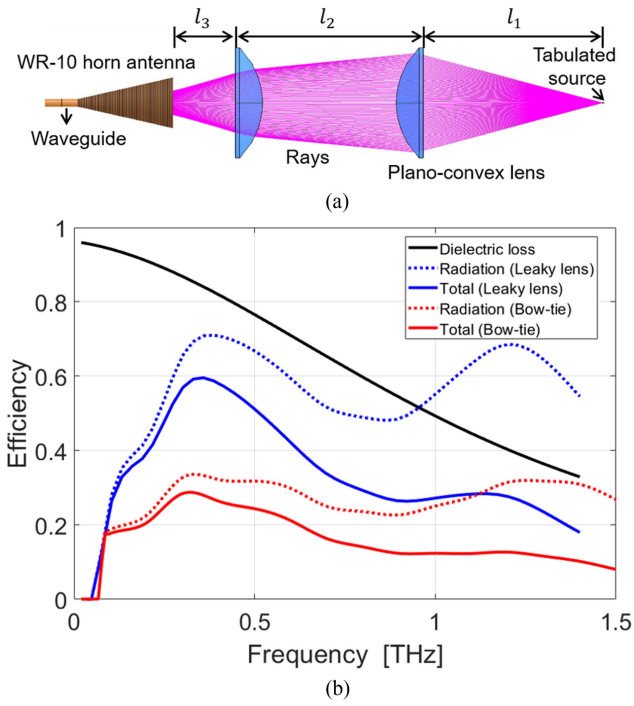

Fig. 6. (a) Simulation setup used in GRASP with ray tracing. (b) Simulated QO channel efficiency.

approximated to evaluate $I_{\text{rad}}(f)$ as constant radiation resistance of 125 Ω. The QO channel was simulated resorting to the PO solver of a commercial software Ticra GRASP [35], and the detailed simulation setup is shown in Fig. 6 with ray tracing. The secondary fields are imported into GRASP as tabulated sauces and are placed behind the first planoconvex lens with the distance $l = 57.35$ mm. Note that l is the summation between the distance l_1, as shown in Fig. 4, the thickness of the entire lens antenna, as depicted in Fig. 1(a), and the phase center distance (15.8 mm below the lens). GRASP then propagates the secondary fields through the two planoconvex lenses to the horn antenna with its PO solver. Finally, the method of moment method analysis is implemented on the horn antenna to obtain the electromagnetic fields inside the waveguide. We can then evaluate the power transmitted inside the waveguide P_d and use it to calculate the efficiency of the channel as $\eta_{qo}(f) = P_d / P_{\text{ant}}$, where P_{ant} is the power radiated by the leaky-lens antenna, as shown in Fig. 1(c). The efficiency of the QO channel $\eta_{qo}(f)$ is shown in Fig. 6(b) as a function of the frequency. The cutoff introduced by the waveguide of the power meter is at 60 GHz [12]. The largest loss is due to the dielectric loss of the two planoconvex lenses, which limits the overall efficiency.

The simulated detected power as a function of the average laser power exciting the antenna for three different bias levels, $V_b = 10, 20, 30$ V, are compared with the corresponding measured power in Fig. 5. The agreement is exceptional, and the differences between the data predicted by the model presented here and the measurement lie within only 1 dB. To clarify why the detected power by the leaky-lens PCA is higher, we plot in Fig. 5 also the radiated power by both PCAs into an infinite silicon medium removing the impact from the QO channel as follows:

$$P_{TX} = 2f_L \int_0^\infty \text{Re}\{Z_a(f)\} |I_{\text{rad}}(f)|^2 df. \quad (2)$$

One can observe that this power is basically the same for both PCAs. Even if this radiated power and the optical setup used to characterize both the leaky-lens and bow–tie PCAs are the same, Fig. 5 shows a higher detected power for the leaky-lens PCA. Thanks to the enhanced broadside radiation because of the presence of air gap between the LT-GaAS membrane and silicon lens (see Fig. 1). The more directive patterns, as shown in Fig. 2, lead to a higher QO channel coupling efficiency [see Fig. 6(b)] and, therefore, higher detected power.

Unfortunately, we are not able to measure beam pattern with our current setup in a similar manner than the one presented in [36] since the beam propagation of the Tera K15 receiver antenna [22] is unknown to us, making it impossible to disentangle the convolution of beam pattern of the emitter and receiver antennas. However, the beam patterns from a leaky-lens antenna are measured thoroughly in [37], where the broadband operation of this type of antenna is shown. We have included detailed simulations of the patterns instead [see Fig. 2(g)–(i)].

VI. Conclusion

The PCA architecture introduced in this work exploits a wideband leaky-lens effect by means of an electrically small air gap between an LT-GaAS membrane and a silicon lens, improving its illumination and the antenna directivity. This results in a better QO efficiency as opposed to standard bow–tie architectures as

the one these authors investigated in [13], even though the QO path used to collect and measure the radiated THz power is the same. The leaky-lens PCA exhibits more directive patterns, and in the present case, the coupling loss along the QO channel is reduced by a factor 2 using the leaky-lens antenna with respect to the bow–tie, leading to a comparable increased in detected power. Although this leaky-lens architecture is more difficult to fabricate than current bow–tie PCAs, we successfully developed a fast and easy fabrication route to make these devices. This fabrication makes the leaky-lens PCA a great candidate when there are constraints on the maximum laser power that can be used, such as commercial TDSS systems with in-fiber laser excitations, where the laser power is limited.

REFERENCES

[1] P. U. Jepsen, D. G. Cooke, and M. Koch, "Terahertz spectroscopy and imaging—Modern techniques and applications," *Laser Photon. Rev.*, vol. 5, no. 1, pp. 124–166, Jan. 2011.

[2] N. Vieweg et al., "Terahertz-time domain spectrometer with 90 dB peak dynamic range," *J. Infrared, Millimeter, Terahertz Waves*, vol. 35, no. 10, pp. 823–832, Oct. 2014.

[3] D. H. Auston, K. P. Cheung, and P. R. Smith, "Picosecond photoconducting Hertzian dipoles," *Appl. Phys. Lett.*, vol. 45, no. 3, pp. 284–286, May 1984.

[4] D. Grischkowsky, S. Keiding, M. van Exter, and C. Fattinger, "Far-infrared time-domain spectroscopy with terahertz beams of dielectrics and semiconductors," *J. Opt. Soc. Amer. B*, vol. 7, no. 10, pp. 2006–2015, Oct. 1990.

[5] P. U. Jepsen, R. H. Jacobsen, and S. R. Keiding, "Generation and detection of terahertz pulses from biased semiconductor antennas," *J. Opt. Soc. Amer. B*, vol. 13, no. 11, pp. 2424–2436, Nov. 1996.

[6] S. Verghese, K. A. McIntosh, and E. R. Brown, "Highly tunable fiber-coupled photomixers with coherent terahertz output power," *IEEE Trans. Microw. Theory Techn.*, vol. 45, no. 8, pp. 1301–1309, Aug. 1997.

[7] M. Tani, S. Matsuura, K. Sakai, and S.-I. Nakashima, "Emission characteristics of photoconductive antennas based on low-temperature-grown GaAs and semi-insulating GaAs," *Appl. Opt.*, vol. 36, no. 30, pp. 7853–7859, 1997.

[8] A. Garufo et al., "A connected array of coherent photoconductive pulsed sources to generate mW average power in the submillimeter wavelength band," *IEEE Trans. THz Sci. Technol.*, vol. 9, no. 3, pp. 221–236, May 2019.

[9] A. Neto, N. L. Juan, and A. Freni, "Time-domain modelling of pulsed photoconducting sources—Part I: The Norton equivalent circuit," *IEEE Trans. Antennas Propag.*, vol. 71, no. 3, pp. 2527–2535, Mar. 2023, doi: 10.1109/TAP.2022.3184517.

[10] B. Globisch, R. J. B. Dietz, D. Stanze, T. Göbel, and M. Schell, "Carrier dynamics in Beryllium doped low-temperature-grown InGaAs/InAlAs," *Appl. Phys. Lett.*, vol. 104, 2014, Art. no. 172103.

[11] H. Roehle et al., "Next generation 1.5 μm terahertz antennas: Mesa-structuring of InGaAs/InAlAs photoconductive layers," *Opt. Express*, vol. 18, pp. 2296–2301, 2010.

[12] A. Garufo et al., "Norton equivalent circuit for pulsed photoconductive antennas—Part II: Experimental validation," *IEEE Trans. Antennas Propag.*, vol. 66, no. 4, pp. 1646–1659, Apr. 2018.

[13] A. F. Bernardis et al., "Time-domain modelling of pulsed photoconducting sources—Part II: Characterization of an LT GaAs bow-tie antenna," *IEEE Trans. Antennas Propag.*, vol. 71, no. 3, pp. 2536–2545, Mar. 2023.

[14] H. Harde and D. Grischkowsky, "Coherent transients excited by subpicosecond pulses of terahertz radiation," *J. Opt. Soc. Amer. B*, vol. 8, pp. 1642–1651, 1991.

[15] N. Katzenellenbogen and D. Grischkowsky, "Efficient generation of 380 fs pulses of THz radiation by ultrafast laser pulse excitation of a biased metal-semiconductor interface," *Appl. Phys. Lett.*, vol. 58, pp. 222–224, 1991.

[16] D. R. Bacon, J. Madéo, and K. M. Dani, "Photoconductive emitters for pulsed terahertz generation," *J. Opt.*, vol. 23, 2021, Art. no. 064001.

[17] N. Llombart and A. Neto, "THz time-domain sensing: The antenna dispersion problem and a possible solution," *IEEE Trans. THz Sci. Technol.*, vol. 2, no. 4, pp. 416–423, Jul. 2012.

[18] A. Neto, "UWB, non dispersive radiation from the planarly fed leaky lens antenna—Part 1: Theory and design," *IEEE Trans. Antennas Propag.*, vol. 58, no. 7, pp. 2238–2247, Jul. 2010, doi: 10.1109/TAP.2010.2048879.

[19] Specialty Coating Systems, 2021. [Online]. Available: https://scscoatings.com

[20] CST Microwave Studio, 2021. [Online]. Available: http://www.cst.com/

[21] H. Zhang, S. O. Dabironezare, G. Carluccio, A. Neto, and N. Llombart, "A Fourier optics tool to derive the plane wave spectrum of quasi-optical systems," *IEEE Antennas Propag. Mag.*, vol. 63, no. 1, pp. 103–116, Feb. 2021, doi: 10.1109/MAP.2020.3027233.

[22] 2023. [Online]. Available: https://www.menlosystems.com/products/thz-antennas-and-components/tera15-fc/

[23] 2023. [Online]. Available: https://www.menlosystems.com/assets/datasheets/THz-Antennas-and-Components/MENLO_TERA15FC-D-EN_2022-02-07_3w.pdf

[24] D. Saeedkia, "Handbook of terahertz technology for imaging, sensing and communications," in *Woodhead Publishing Series in Electronic and Optical Materials*. New York, NY, USA: Elsevier, 2013.

[25] J. Liu et al., "High-Q optomechanical GaAs nanomembranes," *Appl. Phys. Lett.*, vol. 99, 2011, Art. no. 243102.

[26] Y. Uenishi, H. Tanaka, and H. Ukita, "Characterization of AlGaAs microstructure fabricated by AlGaAs/GaAs micromachining," *IEEE Trans. Electron. Devices*, vol. 41, no. 10, pp. 1778–1783, Oct. 1994.

[27] AGC Chemicals, Asahi Glass Co., Ltd., Tokyo, Japan, 2021.

[28] 2021. [Online]. Available: www.ammt.com/products/wet-etching

[29] C. Bryce, "A kinetic study of gallium arsenide etching in H_2O_2-NH_4OH-H_2O solutions," Ph.D. dissertation, Dept. Chem. Eng., McGill Univ., Montreal, QC, Canada, 1996.

[30] 2021. [Online]. Available: https://www.sumipro.nl/

[31] Menlo System GmbH, 2017. [Online]. Available: https://www.menlosystems.com/

[32] Virginia Diodes, Inc., 2017. [Online]. Available: https://www.vadiodes.com/en/

[33] Thorlabs GmbH, 2021. [Online]. Available: https://www.thorlabs.com/

[34] J. M. Khosrofian and B. A. Garetz, "Measurement of a Gaussian laser beam diameter through the direct inversion of knife-edge data," *Appl. Opt.*, vol. 22, pp. 3406–3410, 1983.

[35] GRASP 10.5.0, 2021. [Online]. Available: http://www.ticra.com/software/grasp

[36] M. A. Báez-Chorro, M. Usó-Izquierdo, and B. Vidal, "Accurate beam profile characterization in THz transmission imaging systems," *IEEE Trans. Terahertz Sci. Technol.*, vol. 11, no. 5, pp. 577–582, Sep. 2021.

[37] A. Neto, N. Llombart, J. J. A. Baselmans, A. Baryshev, and S. J. C. Yates, "Demonstration of the leaky lens antenna at submillimeter wavelengths," *IEEE Trans. Terahertz Sci. Technol.*, vol. 4, no. 1, pp. 26–32, Jan. 2014.

Juan Bueno received the Graduate degree from the University of Cantabria, Santander, Spain, in 2003, and the Ph.D. degree from the University of Leiden, Leiden, The Netherlands, in 2007, both in physics.

During his Ph.D. degree studies, he studied quantum crystals at very low temperatures. From 2007 to 2008, he was a Postdoctoral Fellow at the University of California, San Diego, CA, USA, continuing his work on quantum crystals. In 2008, he made the decision to switch research topics and interests from fundamental physics to the study of superconducting devices. He was awarded with a NASA Postdoctoral position, becoming a Postdoctor with Jet Propulsion Laboratory (JPL), USA, until 2010. During this time, he pioneered a new type of pair-breaking radiation detector, the quantum capacitance detector. After his time with JPL, he joined the Center for Astrobiology, Spain, in 2010, after receiving a JAE-doc grant, working mainly on kinetic inductance detectors (KIDs). He became an Instrument Scientist in 2012 with SRON - Netherlands Institute for Space Research, The Netherlands, working on the development of KIDs for submillimeter wave and far IR space-based observatories. He became a high-frequency RF Engineer with ELCA Group, Technical University of Delft, in 2021, working on the XG sensing and communications laboratories. He has authored or coauthored more than 50 peer-reviewed papers, a fourth of them as the first author. His research interest concentrates on the development of over the air technology at submillimeter wave frequencies for detection and communication applications.

Paolo Maria Sberna was born in Palermo, Italy, in 1987. He received the bachelor's degree (cum laude) and the master's degree (cum laude) in physics from the University of Catania, Catania, Italy, in 2009 and 2011, respectively, and the Ph.D. degree in physics from the University of Catania, and NOVA University of Lisbon, Lisbon, Portugal, in 2015.

Since May 2015, he has been with the Delft University of Technology (TU Delft), Delft, The Netherlands. The topic covered during the first two years has been low-temperature Si thin-film transistors fabrication by solution processing. Since 2017, he has been working on III–V photoconductive antennas for terahertz (THz) applications with Terahertz Sensing Group, Microelectronic Department, TU Delft. Since September 2018, he has been Equipment Responsible Scientist with Else Kooi Laboratory, TU Delft. His bachelor's thesis was titled "Bose–Einstein condensation." His master's thesis was titled "Quantum confinement effects on Si nanocrystals observed with Raman spectroscopy." His Ph.D. dissertation was titled "Novel approaches to photoactive nanostructured materials for efficient solar cells." His research interests include solid-state physics, material science, chemistry, and microfabrication.

Arturo Fiorellini-Bernardis (Student Member, IEEE) received the B.Sc. degree in biomedical engineering from the Politecnico di Milano, Milan, Italy, in 2014, the M.Sc. degree (*cum laude*) in electrical engineering from the Delft University of Technology (TU Delft), Delft, The Netherlands, in 2017, and the Ph.D. degree in electrical engineering from Terahertz Sensing Group, Department of Microelectronics, TU Delft.

His research interests include electromagnetic theory as well as the analysis and design of photoconductive antennas for security applications.

Huasheng Zhang (Graduate Student Member, IEEE) received the B.Eng. degree (*cum laude*) in electronic information engineering from Beihang University, Beijing, China, in 2016, and the M.Sc. degree (*cum laude*) in electrical engineering in 2018 from the Delft University of Technology (TU Delft), Delft, The Netherlands, where he is currently working toward the Ph.D. degree in electrical engineering with Terahertz Sensing Group.

His research interests include the design of quasi-optical systems and antenna feeds for next-generation communication and sensing systems.

Andrea Neto (Fellow, IEEE) received the Laurea degree (summa cum laude) in electronic engineering from the University of Florence, Florence, Italy, in 1994, and the Ph.D. degree in electromagnetics from the University of Siena, Siena, Italy, in 2000.

A part of his Ph.D. degree was developed with European Space Agency Research and Technology Center, Noordwijk, The Netherlands. He was with Antenna Section, European Space Agency Research and Technology Center, for over two years. From 2000 to 2001, he was a Postdoctoral Researcher with the California Institute of Technology, Pasadena, CA, USA, where he worked with Submillimeter Wave Advanced Technology Group. From 2002 to January 2010, he was a Senior Antenna Scientist with TNO Defense, Security, and Safety, The Hague, The Netherlands. In February 2010, he became a Full Professor of applied electromagnetism with the Department of Electrical Engineering, Mathematics and Computer Science, Delft University of Technology, Delft, The Netherlands, where he formed and leads the THz Sensing Group. His research interests include the analysis and design of antennas with an emphasis on arrays, dielectric lens antennas, wideband antennas, EBG structures, and THz antennas.

Dr. Neto is a member of the Technical Board of the European School of Antennas and an organizer of the course on antenna imaging techniques. He is also a member of the Steering Committee of the Network of Excellence NEW[1]FOCUS, dedicated to focusing techniques in millimeter and submillimeter[1]wave regimes. He was a recipient of the European Research Council Starting Grant to perform research on advanced antenna architectures for THz sensing systems in 2011, the H. A. Wheeler Award for the best applications paper of 2008 in IEEE TRANSACTIONS ON ANTENNAS AND PROPAGATION, the Best Innovative Paper Prize of the 30th ESA Antenna Workshop in 2008, and the Best Antenna Theory Paper Prize of the European Conference on Antennas and Propagation (EuCAP) in 2010. He served as an Associate Editor for IEEE TRANSACTIONS ON ANTENNAS AND PROPAGATION from 2008 to 2013 and IEEE ANTENNAS AND WIRELESS PROPAGATION LETTERS from 2005 to 2013.

Nuria Llombart (Fellow, IEEE) received the master's and Ph.D. degrees in electrical engineering from the Polytechnic University of Valencia, Valencia, Spain, in 2002 and 2006, respectively.

During her master's degree studies, she spent one year with the Friedrich Alexander University of Erlangen Nuremberg, Erlangen, Germany, and worked with the Fraunhofer Institute for Integrated Circuits, Erlangen, Germany. From 2002 to 2007, she was at Antenna Group, TNO Defense, Security, and Safety Institute, The Hague, The Netherlands, working as a Ph.D. student and afterward as a Researcher. From 2007 to 2010, she was a Postdoctoral Fellow at the California Institute of Technology, working with Submillimeter Wave Advance Technology Group, Jet Propulsion Laboratory, Pasadena, CA, USA. She was a "Ramón y Cajal" Fellow with Optics Department, Complutense University of Madrid, Madrid, Spain, from 2010 to 2012. In September 2012, she joined THz Sensing Group, Technical University of Delft, Delft, The Netherlands, where, as of February 2018, she is a Full Professor. She has coauthored more than 200 journal and international conference contributions in the areas of antennas and THz systems.

Dr. Llombart was the corecipient of H. A. Wheeler Award for the Best Applications Paper of 2008 in IEEE TRANSACTIONS ON ANTENNAS AND PROPAGATION, the 2014 THz Science and Technology Best Paper Award of the IEEE Microwave Theory and Techniques Society, and several NASA awards. She was also the recipient of the 2014 IEEE Antenna and Propagation Society Lot Shafai Mid-Career Distinguished Achievement Award. She serves as a board member of the IRMMW-THz International Society and Associated Editor for IEEE TRANSACTION ON ANTENNAS AND PROPAGATION. In 2015, she was the recipient of European Research Council Starting Grant.